Coherence and quantum Fisher information in general single-qubit parameter estimation processes

Jun-Long Zhao [1,*] Dong-Xu Chen,[1,*] Yu Zhang,[1,2] Yu-Liang Fang,[1] Ming Yang,[3,†]
Qi-Cheng Wu,[1,‡] and Chui-Ping Yang[1,4,§]

[1]*Quantum Information Research Center, Shangrao Normal University, Shangrao 334001, China*
[2]*School of Physics, Nanjing University, Nanjing 210093, China*
[3]*School of Physics and Optoelectronics Engineering, Anhui University, Hefei 230601, China*
[4]*Department of Physics, Hangzhou Normal University, Hangzhou 311121, China*

Quantum metrology is superior to classical metrology in parameter estimation. This is because quantum states have coherence that, however, does not exist in classical states. Previous works were limited to the study of the relationship between quantum Fisher information (QFI) and coherence of the initial probe state only for a specific single-qubit parameter estimation process (e.g., a process described by a single-qubit spin angular momentum operator J_z). Here, we consider a more general case and study the relationship between QFI and coherence of the initial probe state for a single-qubit general parameter estimation process, which is described by a single-qubit spin angular momentum operator $J_{\vec{n}}$ with a general unit vector $\vec{n}$. We find that the QFI is proportional to the square of coherence of the initial probe state, when the single-qubit bases are eigenstates of the spin angular momentum operator $J_{\vec{n}}$ describing the parametrization process. We also design and conduct a linear optical experiment to support our theory. The experimental results are in good agreement with the theoretical ones. This work provides an important guideline for enhancing the precision of parameter estimation.

I. INTRODUCTION

Quantum metrology is essential to improve the estimation precision of unknown physical parameters and consequently crucial for the development of new technologies and fundamental advances [1–3]. Comparing with classical metrology, quantum metrology has received widespread attention for its high estimation precision [4]. This topic has been extensively studied. In general, the whole estimation process can be divided into three steps: preparation of the initial probe state ρ_{in}; evolution of the initial probe state (described by a unitary operator $U(\theta)$ with an unknown parameter θ); and detection of the probe output state $\rho(\theta)$. To estimate an unknown parameter θ, the above process is repeated $N_m \gg 1$ times, and the N_m measurement outcomes are used to construct an optimal unbiased estimator $\hat{\theta}$, such as the maximum likelihood estimator or the Bayesian estimator [5]. In classical parameter estimation cases, N_m probes are employed to independently detect a parameter (N_m is the number of particles or modes, etc.), and the best classical possible scaling is known as standard quantum limit [6,7], whose error scale is $1/N_m$. However, in quantum parameter estimation cases, one can engineer an entangled state of N_m particles as a quantum probe, and the precision scaling can reach to $1/N_m^2$, which is called the Heisenberg limit

[8–10]. When the limitation is reduced, it will lead to a more precise estimation [11].

According to quantum Cramér-Rao inequality [12], the reciprocal of quantum Fisher information (QFI) provides the lower bound on the variance of the estimator θ, i.e., $(\Delta \hat{\theta})^2 \geqslant 1/F_Q$, where $\Delta \hat{\theta}$ is the standard deviation and F_Q is the QFI. Thus, a larger QFI means a higher precision of parameter estimation. In order to reveal the essence of quantum metrology, it is important and necessary to study the relationships between QFI and observable quantities.

The coherent superposition of quantum states represents one of the most fundamental features, which is the distinction of quantum mechanics from the classical realm. This superposition is called quantum coherence, which is an essential ingredient in quantum states and plays important roles in quantum computing, quantum communication, and quantum metrology [13–15]. In 2014, Baumgratz *et al.* [15] established a comprehensive framework of coherence quantification, and the theory has become a method to explore new measures of coherence. Subsequently, some methods have been proposed to quantify quantum coherence, such as the relative entropy [15,16], l_1-norm measure [15,17], skew information [18–20], fidelity based distance measure [21], trace distance [22], quantum correlation [23,24], intrinsic randomness [25], robustness of coherence [26], and so on.

Previous works have shown that QFI can be applied in quantum coherence measure [27–29], and quantum coherence can be used to enhance the precision of parameter estimation owing to quantum coherence effects [20,30–32]. Moreover, the relationship between QFI and coherence has

been investigated over the past years [33–36]. However, we find that Refs. [33–36] studied the relationship between QFI and quantum coherence of the initial probe state in different single-qubit systems, which was only for a specific single-qubit parameter estimation process (e.g., a process described by a single-qubit spin angular momentum operator J_z). In addition, the investigation on the relationship between QFI and coherence is only at the stage of theory up to today.

Motivated by the above, in this work, we will consider a more general case, i.e., we will study the relationship between QFI and coherence of the initial probe state for a general parametrization process, which is described by a single-qubit spin angular momentum operator $J_{\vec{n}}$ with a general unit vector $\vec{n}$. We find that the QFI is a square of coherence of the initial probe state when the single-qubit bases are eigenstates of the spin angular momentum operator $J_{\vec{n}}$ describing the parametrization process. We also design and perform a linear optical experiment to support our theory. The experimental results are in good agreement with the theoretical ones. This work provides an important guideline for enhancing the precision of parameter estimation.

This paper is organized as follows. In Sec. II, we briefly introduce QFI and coherence. The quantitative relationship between QFI and coherence will be studied and presented in Sec. III. In Sec. IV, to support our theory, we design and perform a linear optical experiment, which demonstrates the relationship between QFI and coherence. A brief conclusion is presented in Sec. V.

II. COHERENCE AND QUANTUM FISHER INFORMATION

In general, the variance of the parameter θ is limited by the quantum Cramér-Rao bound [37,38]:

$$\Delta \hat{\theta} \geqslant \Delta \theta_{\text{QCB}} = \frac{1}{\sqrt{N_m F_Q}}, \quad (1)$$

where N_m is the number of the repeated experiments, $\hat{\theta}$ is an unbiased estimator (i.e., a paremeter to be estimated), and the QFI for θ is defined as

$$F_Q = \text{Tr}\big[\rho(\theta)L_\theta^2\big]. \quad (2)$$

Here, $\rho(\theta)$ is the output state when the initial probe state evolves under the parametrization, and L_θ is the so-called symmetric logarithmic derivative, determined by the following equation:

$$\frac{\partial}{\partial \theta}\rho(\theta) = \frac{1}{2}[\rho(\theta)L_\theta + L_\theta \rho(\theta)]. \quad (3)$$

The F_Q in Eq. (2) can be rewritten as [9,39,40]

$$F_Q = \sum_i \frac{(\partial_\theta p_i)^2}{p_i} + 2\sum_{i\neq j} \frac{(p_i - p_j)^2}{p_i + p_j}|\langle \psi_i|\partial_\theta \psi_j\rangle|^2, \quad (4)$$

where $\{|\psi_i\rangle\}$ are the eigenvectors of $\rho(\theta)$ with $\{p_i\}$ being the corresponding eigenvalues. When the parametrization is described by the unitary operator $U(\theta)$, the output state can be written by

$$\rho(\theta) = U(\theta)\rho[U(\theta)]^\dagger, \quad (5)$$

where ρ is an *initial probe state*, $U(\theta) = e^{-i\theta \hat{H}}$, and $\hat{H}$ is a Hermitian Hamiltonian for the parametrization. Because the eigenvalues of ρ and $\rho(\theta)$ are the same, Eq. (4) can be further written as [41–43]

$$F_Q(\rho, \hat{H}) = 2\sum_{i\neq j} \frac{(p_i - p_j)^2}{p_i + p_j}|\langle \phi_i|\hat{H}|\phi_j\rangle|^2, \quad (6)$$

where $\{|\phi_i\rangle\}$ and $\{p_i\}$ are the eigenvectors and the eigenvalues of ρ, respectively. When the initial probe state is a pure state, Eq. (6) becomes [41–43]:

$$F_Q(\rho, \hat{H}) = 4(\langle \hat{H}^2\rangle - \langle \hat{H}\rangle^2). \quad (7)$$

In the present work, we consider a single-qubit parametrization process where the qubit acts as a probe. For a single-qubit system, a generic Hamiltonian characterizing the parametrization can be written as

$$\hat{H} = \Omega J_{\vec{n}}, \quad (8)$$

where the Ω denotes an energy scale and the $J_{\vec{n}}$ is a pseudospin angular momentum operator, given by

$$J_{\vec{n}} = \sum_{\alpha=x,y,z} \frac{1}{2} n_\alpha \sigma_\alpha = \frac{1}{2}\vec{n}\cdot\vec{\sigma}. \quad (9)$$

Here, σ_α ($\alpha = x, y, z$) are the Pauli matrices and $\vec{n} = (n_x, n_y, n_z)$ is a direction unit vector. After replacing $\hat{H}$ with $\Omega J_{\vec{n}}$, Eq. (6) is simplified as

$$F_Q(\rho, \hat{H}) = \Omega^2 F_Q(\rho, J_{\vec{n}}), \quad (10)$$

with

$$F_Q(\rho, J_{\vec{n}}) = 2\sum_{i\neq j} \frac{(p_i - p_j)^2}{p_i + p_j}|\langle \phi_i|J_{\vec{n}}|\phi_j\rangle|^2. \quad (11)$$

We now introduce the measure of coherence for general bases. Generally speaking, coherence measure includes two parts, i.e., quantum state and measure basis. Baumgaratz *et al.* defined a coherence measure in terms of the norm of off-diagonal elements [15]. Consider an initial probe state ρ and a basis $K := \{|i\rangle\}$. The coherence of this state is defined as [15]

$$C_K(\rho) = \sum_{i\neq j} |\langle i|\rho|j\rangle|. \quad (12)$$

In a single-qubit system, Mani and Karimipour [17] defined a simple coherence measure based on Eq. (12). For an arbitrary quantum state of a single qubit, the density operator can be expressed as $\rho = (I + \vec{r}\cdot\vec{\sigma})/2$, where $\vec{r}$ is Bloch vector of ρ. If one chooses the basis of the qubit as the eigenstates of $J_{\vec{n}}$, the coherence of the state can be written as [17]

$$C_{\vec{n}}(\rho) = r\sqrt{1 - (\vec{e}_r \cdot \vec{n})^2}, \quad (13)$$

where $\vec{e}_r$ is the unit vector $\frac{\vec{r}}{r}$. To see this more clearly, let us consider several examples. For $\vec{n} = (0, 0, 1)$, $\vec{n} = (1, 0, 0)$, and $\vec{n} = (0, 1, 0)$, we have $J_{\vec{n}} = J_z$, $J_{\vec{n}} = J_x$, and $J_{\vec{n}} = J_y$, respectively. Therefore, for these three cases, the base involved in Eq. (13) is chosen as eigenstates of $J_{\vec{n}} = J_z = \sigma_z/2$, $J_{\vec{n}} = J_x = \sigma_x/2$, and $J_{\vec{n}} = J_y = \sigma_y/2$, respectively.
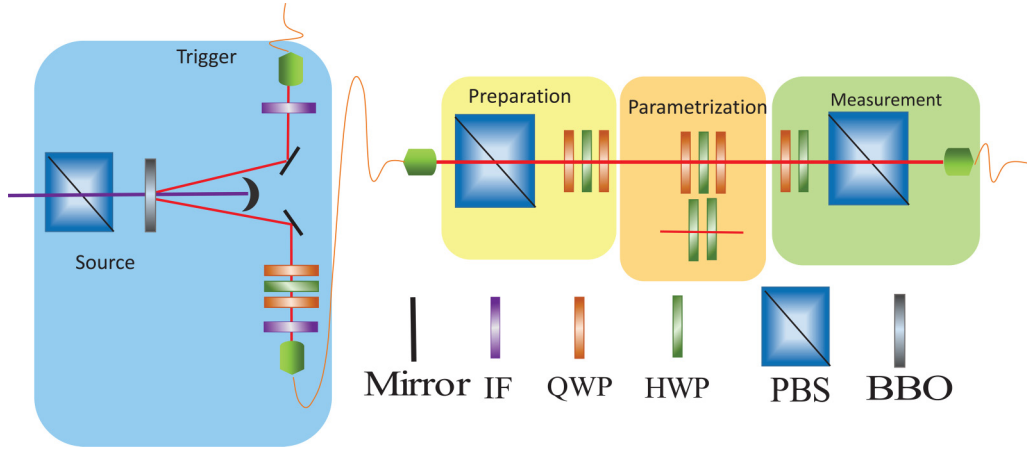
FIG. 1. Experimental setup. Blue area: generation of single-photon source. Yellow area: preparation of the initial probe state. Orange area: parametrization process of the probe state. Green area: measurement of output states. Here, the optical elements HWP, QWP, PBS, and BBO are acronyms of half-wave plate, quarter-wave plate, polarization beam splitter, and β-barium borate, respectively.

III. RELATIONSHIP BETWEEN COHERENCE AND QUANTUM FISHER INFORMATION

In this section, we will prove the relationship between QFI and coherence of the initial probe state for a general parametrization process. Generally, an arbitrary single-qubit state can be written in the Bloch sphere as

$$\rho = \tfrac{1}{2}(I + \vec{r} \cdot \vec{\sigma}), \qquad (14)$$

where $\vec{r} = (r_x, r_y, r_z)$ is the Bloch vector. Based on the spherical coordinates, we assume

$$r_x = r \sin\varphi \cos\phi, \quad r_y = r \sin\varphi \sin\phi, \quad r_z = r \cos\varphi. \qquad (15)$$

Based on Eq. (6), one can easily find that when the initial probe state is Eq. (14), the QFI in the parametrization is given by

$$\begin{aligned}
F_Q(\rho, \hat{H}) &= 4(p_1 - p_2)^2 |\langle \phi_1 | \hat{H} | \phi_2 \rangle|^2 \\
&= 4(p_1 - p_2)^2 |\langle \phi_1 | \Omega J_{\vec{n}} | \phi_2 \rangle|^2 \\
&= F_Q(\rho, J_{\vec{n}})\Omega^2,
\end{aligned} \qquad (16)$$

with

$$F_Q(\rho, J_{\vec{n}}) = 4(p_1 - p_2)^2 |\langle \phi_1 | J_{\vec{n}} | \phi_2 \rangle|^2. \qquad (17)$$

After a derivation (see Appendix A), we obtain from Eq. (17)

$$F_Q(\rho, J_{\vec{n}}) = r^2 [1 - (\vec{e}_r \cdot \vec{n})^2]. \qquad (18)$$

According to Eq. (13), one can see that Eq. (18) can be further written as

$$F_Q(\rho, J_{\vec{n}}) = C_{\vec{n}}^2(\rho). \qquad (19)$$

Substituting Eq. (19) into Eq. (16), we have

$$F_Q(\rho, \hat{H}) = (C_{\vec{n}})^2 \Omega^2, \qquad (20)$$

which shows that the QFI is proportional to the square of coherence of the initial probe state when the bases are chosen as eigenstates of the spin angular momentum operator $J_{\vec{n}}$ with a general unit vector $\vec{n}$, which describes the parametrization process in a single-qubit system.
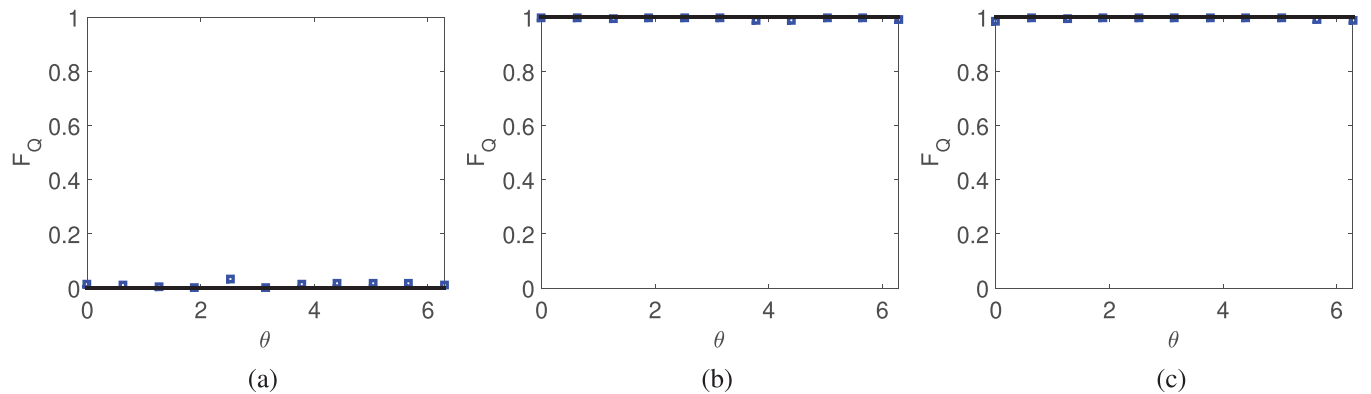

FIG. 2. The QFI varies with the estimated parameter θ in the case when the initial probe state $(|H\rangle + |V\rangle)/\sqrt{2}$ evolves under different parametrization processes. (a), (b), and (c) correspond to the parametrization processes U_x, U_y, and U_z, respectively. Solid curves denote theoretical values while squares are experimental data.
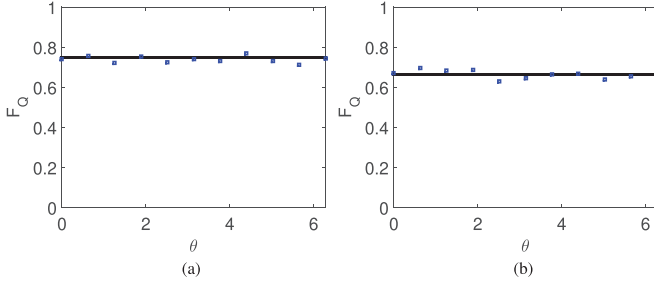
FIG. 3. The QFI varies with the estimated parameter θ in the case when the initial probe state $1/\sqrt{2}(|H\rangle + |V\rangle)$ evolves under different parametrization processes. (a) and (b) correspond to the parametrization processes U_1 and U_2, respectively. Solid curves denote theoretical values while squares are experimental data.

IV. EXPERIMENTAL DEMONSTRATION

In the previous section, we have derived Eq. (20), which gives the relationship between QFI and coherence of the initial probe state for the general parametrization process. We now design a linear optical experiment to verify this relationship. For simplicity, we set $\Omega = 1$, i.e., Eq. (20) reduces to Eq. (19).

A. Experimental setup

As depicted in Fig. 1, the experimental setup includes four parts: generation of single-photon source, preparation of the initial probe state, parametrization process, and state detection. The single-photon source is generated through a spontaneous parametric down-conversion process by pumping a nonlinear β-barium-borate (BBO) crystal with a 404-nm pump laser via type-II phase matching. After photons pass through the 10-nm interference filter (IF), one photon serves as a trigger while the other signal photon is used as the probe photon. Because of the disturbance of the single-mode fiber to polarization, the probe photon needs to pass through the sandwich structure (QWP-HWP-QWP) to eliminate this influence, and then goes through various optical elements. Here, QWP represents "quarter-wave plate" while HWP represents "half-wave plate." An arbitrary initial probe state can be prepared by a combination of two QWPs and one HWP.

In the experiment, we consider three different initial probe states $|H\rangle$, $(|H\rangle + |V\rangle)/\sqrt{2}$, and $(\sqrt{3}|H\rangle + |V\rangle)/2$. The three states are prepared by using a HWP with angles of $0°$, $22.5°$, and $15°$, respectively. Here $|H\rangle$ and $|V\rangle$ denote the horizontal and vertical polarization states, respectively. We choose three kinds of different parametrization processes, which are described by the following unitary operators [44]:

$$U_x(\theta) = e^{-iJ_x\theta}, \tag{21}$$

$$U_y(\theta) = e^{-iJ_y\theta}, \tag{22}$$

$$U_z(\theta) = e^{-iJ_z\theta}. \tag{23}$$

To investigate the sensitivity of the output state to the estimated parameter θ, different parameters θ are applied in the parametrization process. The unitary operators in Eqs. (21)–(23) are implemented using a combination of QWPs and HWPs as follows:

$$U_x(\theta) = R_{QWP}(0°)R_{HWP}(\pi/2 - \theta/4)R_{QWP}(0°), \tag{24}$$

$$U_y(\theta) = R_{HWP}\left(\frac{\theta}{4}\right)R_{HWP}(0°), \tag{25}$$

$$U_z(\theta) = R_{QWP}(45°)R_{HWP}\left(\frac{\theta + \pi}{4}\right)R_{QWP}(45°). \tag{26}$$

For the details on Eqs. (24)–(26), see Appendix B, where R_{HWP} and R_{QWP} represent unitary transformations of HWP and QWP. In addition, the linear superposition of J_x, J_y, and J_z has been studied for the following two cases: $\vec{n}_1 = (1/2, 1/2, \sqrt{1/2})$ and $\vec{n}_2 = (\sqrt{1/3}, \sqrt{1/3}, \sqrt{1/3})$. The corresponding unitary operators can be expressed as follows:

$$U_1 = e^{-iJ_{\vec{n}_1}\theta}, \tag{27}$$

$$U_2 = e^{-iJ_{\vec{n}_2}\theta}, \tag{28}$$

where

$$J_{\vec{n}_1} = \frac{1}{2}\left(\frac{1}{2}\sigma_x + \frac{1}{2}\sigma_y + \frac{1}{\sqrt{2}}\sigma_z\right), \tag{29}$$

$$J_{\vec{n}_2} = \frac{1}{2}\left(\frac{1}{\sqrt{3}}\sigma_x + \frac{1}{\sqrt{3}}\sigma_y + \frac{1}{\sqrt{3}}\sigma_z\right). \tag{30}$$
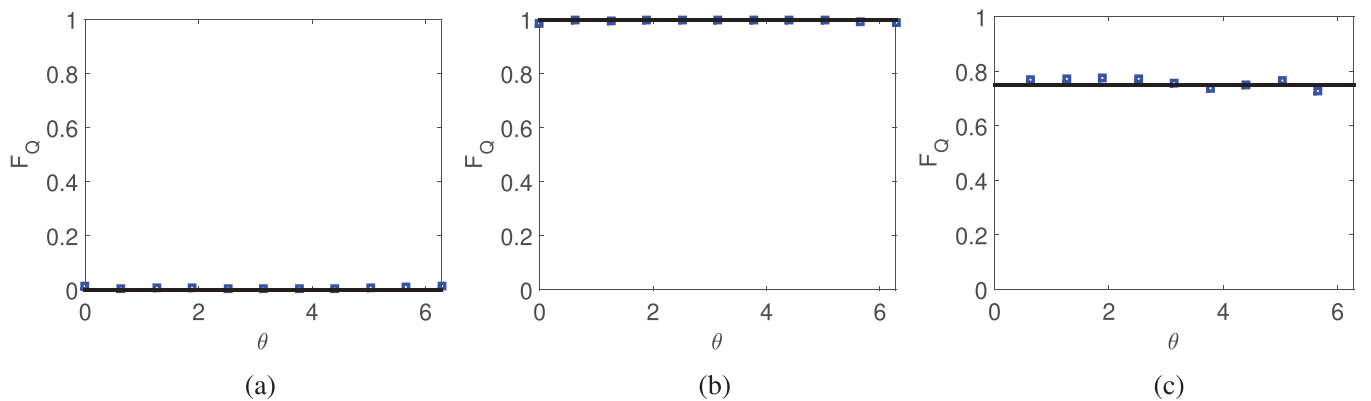

FIG. 4. The QFI varies with the estimated parameter θ in the case when different initial probe states evolve under the same parametrization process U_z. (a), (b), and (c) correspond to the initial probe states $|H\rangle$, $(|H\rangle + |V\rangle)/\sqrt{2}$, and $(\sqrt{3}|H\rangle + |V\rangle)/2$, respectively. Solid curves denote theoretical values while squares are experimental data.

TABLE I. The experimental values of QFI and the theoretical values of coherence when the initial probe state is $(|H\rangle + |V\rangle)/\sqrt{2}$. C_{probe} represents coherence.

Parametrization	QFI_{exp}	C_{probe}	C_{probe}^2
U_x	0.012 ± 0.010	0	0
U_y	0.997 ± 0.002	1	1
U_z	0.996 ± 0.004	1	1

In an optical system, the U_1 and U_2 can be implemented by the combinations of QWP-HWP-QWP.

Lastly, the output state is measured through the coincidence count of photons in four measurement bases $\{|H\rangle, |V\rangle, |R\rangle = (|H\rangle - i|V\rangle)/\sqrt{2}, |D\rangle = (|H\rangle + |V\rangle)/\sqrt{2}\}$. The four measurement bases are implemented by a combination of QWP, HWP, and PBS. Here, PBS is the acronym for polarization beam splitter. To realize these four bases, the angles of QWP and HWP are chosen as $(0°, 0°)$, $(0°, 45°)$, $(0°, 22.5°)$, and $(45°, 22.5°)$, respectively. The experimental QFI can be calculated from the measurement results (see Appendix C for details).

B. Experimental results and analyses

Next, we will experimentally study the relationship between QFI and coherence of the initial probe state during the parametrization process. Our study includes two cases: (1) the same initial probe state but different parametrization processes (Figs. 2 and 3) and (2) different initial probe states but the same parametrization process (Fig. 4).

For the first case, we choose the initial probe state $(|H\rangle + |V\rangle)/\sqrt{2}$ and consider three different parametrization processes U_x, U_y, and U_z. As mentioned previously, the spin angular momentum operators, associated with these three parametrization processes, are J_x, J_y, and J_z. Figures 2(a), 2(b), and 2(c) show the dynamics of QFIs with the parameter θ for the three parametrization processes. Meanwhile, Figs. 3(a) and 3(b) show the dynamics of QFIs with the parameter θ for the two parametrization processes.

From Figs. 2(a), 2(b), and 2(c), we find that for the three parametrization processes U_x, U_y, and U_z, the average values of QFIs are equal to 0.012, 0.997, and 0.996, with deviations 0.010, 0.002, and 0.004, respectively. Meanwhile, when the initial probe state considered here is expanded in terms of the eigenstates of the spin angular momentum operators J_x, J_y, and J_z, the coherence of the initial probe state is equal to 0, 1, and 1, respectively. Thus, for the three parametrization processes U_x, U_y, and U_z, the relationship between QFI and the coherence of the initial probe state fits well with the

TABLE II. The experimental values of QFI and the theoretical values of coherence when the initial probe state is $(|H\rangle + |V\rangle)/\sqrt{2}$. C_{probe} represents coherence.

Parametrization	QFI_{exp}	C_{probe}	C_{probe}^2
U_1	0.7396 ± 0.0164	$\frac{\sqrt{3}}{2}$	$\frac{3}{4}$
U_2	0.6641 ± 0.0206	$\frac{\sqrt{6}}{3}$	$\frac{2}{3}$

TABLE III. The experimental values of QFI and the theoretical values of coherence for the parametrization process U_z.

Initial probe states	QFI_{exp}	C_{probe}	C_{probe}^2
$|H\rangle$	0.007 ± 0.003	0	0
$(|H\rangle + |V\rangle)/\sqrt{2}$	0.996 ± 0.004	1	1
$(\sqrt{3}|H\rangle + |V\rangle)/2$	0.759 ± 0.016	$\sqrt{3}/2$	0.75

relationship described by Eq. (20) (with $\Omega = 1$ set above). See Table I. From Figs. 3(a) and 3(b), we find that for the two parametrization processes U_1 and U_2, the average values of QFIs are equal to 0.7396 and 0.6641, with deviations 0.0164 and 0.0206, respectively. Meanwhile, when the initial probe state considered here is expanded in terms of the eigenstates of the spin angular momentum operators $J_{\bar{n}_1}$ and $J_{\bar{n}_2}$, the coherence of the initial probe state is equal to $\frac{\sqrt{3}}{2}$ and $\frac{\sqrt{6}}{3}$, respectively. Thus, for the two parametrization processes U_1 and U_2, the relationship between QFI and the coherence of the initial probe state basically fits with the relationship described by Eq. (20) (with $\Omega = 1$ set above). See Table II.

For the second case, we choose three different initial probe states $|H\rangle$, $(|H\rangle + |V\rangle)/\sqrt{2}$, and $(\sqrt{3}|H\rangle + |V\rangle)/2$, and consider the same parametrization process described by the operator U_z. Figures 4(a)–4(c) show the dynamics of QFIs with the parameter θ for the three initial probe states under the same parametrization process U_z. From Fig. 4, the experimental average values of QFI for the three initial probe states are 0.007, 0.996, and 0.759, with deviations 0.003, 0.004, and 0.016, respectively. Meanwhile, a simple calculation finds that when the three initial probe states are expanded in the eigenstates $|H\rangle$ and $|V\rangle$ of J_z, their coherences are 0, 1, and $\sqrt{3}/2$. The experimental values of QFI and the theoretical values of coherences are listed in Table III.

From Table III, we find that the experimental value of QFI approximately equals the square of the coherence of the corresponding initial probe state within the allowable error range. This indicates that the result obtained here is in agreement with Eq. (20).

According to the results obtained for the two cases above, it can be concluded that within the allowable error range, the experimental results are consistent with the theoretical results of Eq. (20). Therefore, we have experimentally verified that the QFI and the coherence of the initial probe state under the eigenstate base of $J_{\bar{n}}$ has a quantitative relationship as described in Eq. (20).

In the experiment, we take three samples from each test point, but the fluctuation between the three samples itself is small and the experimental data volatility is not obvious in the graphs. Thus, we directly take the average in the data processing, without drawing the error bars in the graphs for simplicity.

V. CONCLUSION

We have studied the relationship between QFI and coherence of the initial probe state for a single-qubit general parameter estimation process. We found that this relationship can be expressed as the formula of Eq. (20), which shows that the QFI is proportional to the square of coherence of the

initial probe state when the bases are eigenstates of a spin angular momentum operator $J_{\vec{n}}$ describing the parametrization process. This work is a significant generalization of the previous works which only studied the relationship between QFI and coherence of the initial probe state for a specific parametrization process. To support our theory, we have designed and performed a linear optical experiment. The experimental results fit well with the theoretical results. Our experiment demonstrated the relationship between QFI and coherence of the initial probe state. The results obtained in this work provide a profound insight on the enhancement of the precision of parameter estimation and may have applications in quantum information science and technology.

APPENDIX A: DERIVATION OF EQ. (18)

The eigenvalues and eigenvectors of ρ [Eq. (14)] can be written as

$$p_1 = \frac{1+r}{2}, \quad p_2 = \frac{1-r}{2}, \tag{A1}$$

$$|\phi\rangle_1 = \begin{pmatrix} \cos\frac{\varphi}{2} \\ \sin\frac{\varphi}{2}e^{i\phi} \end{pmatrix}, \quad |\phi\rangle_2 = \begin{pmatrix} \sin\frac{\varphi}{2} \\ -\cos\frac{\varphi}{2}e^{i\phi} \end{pmatrix}. \tag{A2}$$

According to Eqs. (9) and (A2), one has

$$
\begin{aligned}
\langle\phi_1|J_{\vec{n}}|\phi_2\rangle &= \frac{1}{2}\left(\cos\frac{\varphi}{2} \ \sin\frac{\varphi}{2}e^{-i\phi}\right)(n_x\sigma_x + n_y\sigma_y + n_z\sigma_z)\begin{pmatrix} \sin\frac{\varphi}{2} \\ -\cos\frac{\varphi}{2}e^{i\phi} \end{pmatrix} \\
&= \frac{1}{2}\left(\cos\frac{\varphi}{2} \ \sin\frac{\varphi}{2}e^{-i\phi}\right)\begin{pmatrix} 1+n_z & n_x - in_y \\ n_x - in_y & n_x - in_y \end{pmatrix}\begin{pmatrix} \sin\frac{\varphi}{2} \\ -\cos\frac{\varphi}{2}e^{i\phi} \end{pmatrix} \\
&= \frac{1}{2}\left[(1+n_z)\cos\frac{\varphi}{2}\sin\frac{\varphi}{2} + (n_x + in_y)\sin^2\frac{\varphi}{2}e^{-i\phi} - (n_x - in_y)\cos^2\frac{\varphi}{2}e^{i\phi} - (1-n_z)\cos\frac{\varphi}{2}\sin\frac{\varphi}{2}\right] \\
&= \frac{1}{2}\left[2n_z\cos\frac{\varphi}{2}\sin\frac{\varphi}{2} + \sin^2\frac{\varphi}{2}(n_x\cos\phi - in_x\sin\phi + in_y\cos\phi + n_y\sin\phi) \right. \\
&\quad \left. - \cos^2\frac{\varphi}{2}(n_x\cos\phi + in_x\sin\phi - in_y\cos\phi + n_y\sin\phi)\right] \\
&= \frac{1}{2}[n_z\sin\varphi - n_x\cos\phi\cos\varphi - n_y\cos\varphi\sin\phi + i(-n_x\sin\phi + n_y\cos\phi)]. \tag{A3}
\end{aligned}
$$

After inserting Eqs. (A1) and (A3) into Eq. (17), we obtain

$$
\begin{aligned}
F_Q(\rho, J_{\vec{n}}) &= 4(p_1 - p_2)^2|\langle\phi_1|J_{\vec{n}}|\phi_2\rangle|^2 \\
&= r^2\left[(n_z\sin\varphi - n_x\cos\phi\cos\varphi - n_y\cos\varphi\sin\phi)^2 + (-n_x\sin\phi + n_y\cos\phi)^2\right] \\
&= r^2\left[n_z^2\sin^2\varphi + n_x^2\cos^2\phi\cos^2\varphi + n_y^2\cos^2\varphi\sin^2\phi - 2n_xn_z\sin\varphi\cos\varphi\cos\phi - 2n_yn_z\sin\varphi\cos\varphi\sin\phi \right. \\
&\quad \left. + 2n_xn_y\cos^2\varphi\cos\phi\sin\phi + n_x^2\sin^2\phi + y^2\cos\phi - 2n_xn_y\sin\phi\cos\phi\right] \\
&= r^2\left[(\cos^2\phi\cos^2\varphi + \sin^2\phi)n_x^2 + (\cos^2\phi + \cos^2\varphi\sin^2\phi)n_y^2 + n_z^2\sin^2\varphi \right. \\
&\quad \left. + 2(\cos^2\varphi\cos\phi\sin\phi - \sin\phi\cos\phi)n_xn_y - 2\sin\varphi\cos\varphi\cos\phi n_xn_z - 2\sin\varphi\cos\varphi\sin\phi n_yn_z\right] \\
&= r^2\left[(1 - \sin^2\varphi\cos^2\phi)n_x^2 + (1 - \sin^2\varphi\sin^2\phi)n_y^2 + (1 - \cos^2\varphi)n_z^2 \right. \\
&\quad \left. - 2\sin^2\varphi\cos\phi\sin\phi n_xn_y - 2\sin\varphi\cos\varphi\cos\phi n_xn_z - 2\sin\varphi\cos\varphi\sin\phi n_yn_z\right] \\
&= r^2\left[n_x^2 + n_y^2 + n_z^2 - (\sin\varphi\cos\phi n_x + \sin\varphi\sin\phi n_y + \cos\varphi n_z)^2\right] \\
&= r^2[1 - (\vec{e}_r \cdot \vec{n})^2], \tag{A4}
\end{aligned}
$$

which is Eq. (18) in the main text.

APPENDIX B: DERIVATION OF EQS. (24)–(26)

In the main text, the parametrization processes are U_x, U_y, and U_z, respectively. They are described by

$$
\begin{aligned}
U_x(\theta) &= e^{-iJ_x\theta}, \\
U_y(\theta) &= e^{-iJ_y\theta}, \\
U_z(\theta) &= e^{-iJ_z\theta}, \tag{B1}
\end{aligned}
$$

with

$$J_x = \tfrac{1}{2}\sigma_x, \qquad J_y = \tfrac{1}{2}\sigma_y, \qquad J_z = \tfrac{1}{2}\sigma_z. \tag{B2}$$

Substituting Eq. (B2) into Eq. (B1), the unitary operators in Eq. (B1) take the following matrices:

$$U_x(\theta) = \begin{pmatrix} \cos\frac{\theta}{2} & -i\sin\frac{\theta}{2} \\ -i\sin\frac{\theta}{2} & \cos\frac{\theta}{2} \end{pmatrix}, \tag{B3}$$

$$U_y(\theta) = \begin{pmatrix} \cos\frac{\theta}{2} & -\sin\frac{\theta}{2} \\ \sin\frac{\theta}{2} & \cos\frac{\theta}{2} \end{pmatrix}, \tag{B4}$$

$$U_z(\theta) = \begin{pmatrix} e^{-i\theta/2} & 0 \\ 0 & e^{i\theta/2} \end{pmatrix}. \tag{B5}$$

Meanwhile, the unitary transformations, performed through QWP and HWP, are described by

$$R_{\text{QWP}}(\alpha) = \begin{pmatrix} \cos^2\alpha + i\sin^2\alpha & \sin\alpha\cos\alpha(1-i) \\ \sin\alpha\cos\alpha(1-i) & \sin^2\alpha + i\cos^2\alpha \end{pmatrix}, \tag{B6}$$

$$R_{\text{HWP}}(\beta) = \begin{pmatrix} \cos 2\beta & \sin 2\beta \\ \sin 2\beta & -\cos 2\beta \end{pmatrix}. \tag{B7}$$

According to Eqs. (B6) and (B7), we have

$$R_{\text{QWP}}(0°) = \begin{pmatrix} 1 & 0 \\ 0 & i \end{pmatrix}, \tag{B8}$$

$$R_{\text{QWP}}(45°) = \frac{1}{\sqrt{2}} \begin{pmatrix} i & 1 \\ 1 & i \end{pmatrix}, \tag{B9}$$

$$R_{\text{HWP}}(\beta) = \begin{pmatrix} \cos 2\beta & \sin 2\beta \\ \sin 2\beta & -\cos 2\beta \end{pmatrix}. \tag{B10}$$

Thus, we obtain

$$R_{\text{QWP}}(0°)R_{\text{HWP}}(\beta)R_{\text{QWP}}(0°) = \begin{pmatrix} \cos 2\beta & i\sin 2\beta \\ i\sin 2\beta & \cos 2\beta \end{pmatrix}, \tag{B11}$$

$$R_{\text{QWP}}(45°)R_{\text{HWP}}(\beta)R_{\text{QWP}}(45°) = \begin{pmatrix} e^{(\pi-2\beta)i} & 0 \\ 0 & e^{2\beta i} \end{pmatrix}, \tag{B12}$$

$$R_{\text{HWP}}(\beta)R_{\text{HWP}}(0°) = \begin{pmatrix} \cos 2\beta & -\sin 2\beta \\ \sin 2\beta & \cos 2\beta \end{pmatrix}. \tag{B13}$$

Comparing Eq. (B11) with Eq. (B3), we have

$$U_x(\theta) = R_{\text{QWP}}(0°)R_{\text{HWP}}(\pi/2 - \theta/4)R_{\text{QWP}}(0°). \tag{B14}$$

Next, comparing Eq. (B13) with Eq. (B4), we obtain

$$U_y(\theta) = R_{\text{HWP}}\left(\frac{\theta}{4}\right)R_{\text{HWP}}(0°). \tag{B15}$$

Last, by comparing Eq. (B12) with Eq. (B5), it is easy to find

$$U_z(\theta) = R_{\text{QWP}}(45°)R_{\text{HWP}}\left(\frac{\theta+\pi}{4}\right)R_{\text{QWP}}(45°). \tag{B16}$$

Equations (B14)–(B16) here are exactly Eqs. (24)–(26) in the main text.

Note that the functions of both the operators U and $e^{i\theta}U$ are identical. This is because the states $U|\psi\rangle$ and $e^{i\theta}U|\psi\rangle$ are the same due to the principles of quantum mechanics. Thus, the overall phases in Eqs. (B8)–(B16) are neglected.

APPENDIX C: THE EXPERIMENTAL VALUE OF QFI

The QFI can be calculated via Eq. (4) in the main text. The parametrization process is governed by $U_\theta = e^{-i\hat{H}\theta}$, and $\hat{H}$ is a Hermitian Hamiltonian for the parametrization. Thus, we have

$$U(\theta) = e^{-i\hat{H}\theta}. \tag{C1}$$

Suppose the initial probe state is ρ. Thus, we have

$$\rho(\theta) = U(\theta)\rho[U(\theta)]^\dagger. \tag{C2}$$

In general, a quantum state can be expressed as

$$\rho = \sum p_i|\psi_i\rangle\langle\psi_i|. \tag{C3}$$

Based on Eqs. (C1)–(C3), we have

$$\rho(\theta) = \sum p_i|\psi_i(\theta)\rangle\langle\psi_i(\theta)|, \tag{C4}$$

where

$$|\psi_i(\theta)\rangle = U(\theta)|\psi_i\rangle. \tag{C5}$$

Thus,

$$\partial_\theta p_i = 0, \tag{C6}$$

$$|\partial_\theta\psi_i\rangle = -i\hat{H}|\psi_i(\theta)\rangle. \tag{C7}$$

Substituting Eqs. (C6) and (C7) into Eq. (4) of the main text, the QFI can be expressed as

$$F_Q = 2\sum_{i\neq j}\frac{(p_i-p_j)^2}{p_i+p_j}|\langle\psi_i(\theta)|\hat{H}|\psi_j(\theta)\rangle|^2. \tag{C8}$$

When the probe quantum state is a single-qubit pure state and the Hermite Hamiltonian for the parametrization is a single-qubit spin angular momentum operator $J_{\vec{n}}$ with a general unit vector $\vec{n}$, Eq. (C8) can be expressed as

$$F_Q(\theta) = 4\big(\text{Tr}\big[\rho(\theta)J_{\vec{n}}^2\big] - \{\text{Tr}[\rho(\theta)J_{\vec{n}}]\}^2\big). \tag{C9}$$

Equation (C9) is used to calculate the experimental value of the QFI in this work.

---

[1] L. Pezzè, A. Smerzi, M. K. Oberthaler, R. Schmied, and P. Treutlein, Quantum metrology with nonclassical states of atomic ensembles, Rev. Mod. Phys. **90**, 035005 (2018).

[2] V. Giovannetti, S. Lloyd, and L. Maccone, Advances in quantum metrology, Nat. Photonics **5**, 222 (2011).

[3] R. Demkowicz-Dobrzański, M. Jarzyna, and J. Kolodyński, Chapter Four-Quantum Limits in Optical Interferometry, Prog. Opt. **60**, 345 (2015).

[4] D. R. Cox and D. V. Hinkley, *Theoretical Staristics* (Chapman and Hall, London, 1974), Chap. 8.

[5] Y. Ma, M. Pang, L. Chen, and W. Yang, Improving quantum parameter estimation by monitoring quantum trajectories, Phys. Rev. A **99**, 032347 (2019).

[6] V. B. Braginsky and Y. I. Vorontsov, Quantum-mechanical limitations in macroscopic experiments and modern experimental technique, Sov. Phys. Usp. **17**, 644 (1975).

[7] V. Giovannetti, S. Lloyd, and L. Maccone, Quantum-enhanced measurements: Beating the standard quantum limit, Science **306**, 1330 (2004).

[8] V. Giovannetti, S. Lloyd, and L. Maccone, Quantum Metrology, Phys. Rev. Lett. **96**, 010401 (2006).

[9] L. Pezzé and A. Smerzi, Entanglement Nonlinear Dynamics, and the Heisenberg Limit, Phys. Rev. Lett. **102**, 100401 (2009).

[10] L. Pezzé, Sub-Heisenberg phase uncertainties, Phys. Rev. A **88**, 060101(R) (2013).

[11] S. M. Roy and S. M. Braunstein, Exponentially Emhanced Quantum Metrology, Phys. Rev. Lett. **100**, 220501 (2008).

[12] H. Cramér, *Mathematical Mathods of Statistics* (Princeton University, Princeton, NJ, 1946), p. 500.

[13] R. J. Glauber, Coherent and incoherent state of the radiation field, Phys. Rev. **131**, 2766 (1963).

[14] E. C. G. Sudarshan, Equivalence of Semiclassical and Quantum Mechanical Descriptions of Statistical Light Beams, Phys. Rev. Lett. **10**, 277 (1965).

[15] T. Baumgratz, M. Cramer, and M. B. Plenio, Quantifying Coherence, Phys. Rev. Lett. **113**, 140401 (2014).

[16] H. Q. Zhao and C. S. Yu, Coherence measure in terms of the Tsallis relative α entropy, Sci. Rep. **8**, 299 (2018).

[17] A. Mani and V. Karimipour, Cohering and decohering power of quantum channels, Phys. Rev. A **92**, 032331 (2015).

[18] D. Girolami, Observable Measure of Quantum Coherence in Finite Dimensional Systems, Phys. Rev. Lett. **113**, 170401 (2014).

[19] E. P. Wigner and M. M. Yanase, Information contents of distributions, Proc. Natl. Acad. Sci. U.S.A. **49**, 910 (1963).

[20] D. P. Pires, L. C. Céleri, and P. O. Soares-Pinto, Geometric lower bound for a quantum coherence measure, Phys. Rev. A **91**, 042330 (2015).

[21] L. H. Shao, Z. J. Xi, H. Fan, and Y. M. Li, Fidelity and trace-norm distances for quantifying coherence, Phys. Rev. A **91**, 042120 (2015).

[22] S. Rana, P. Parashar, and M. Lewenstein, Trace-distance measure of coherence, Phys. Rev. A **93**, 012110 (2016).

[23] A. Streltos, U. Singh, H. S. Dhar, M. N. Bera, and G. Adesso, Measuring Quantum Coherence with Entanglement, Phys. Rev. Lett. **115**, 020403 (2015).

[24] J. J. Ma, B. Yadin, D. Girolami, V. Vedral, and M. Gu, Converting Coherence to Quantum Correlations, Phys. Rev. Lett. **116**, 160407 (2016).

[25] X. Yuan, H. Zhou, Z. Cao, and X. F. Ma, Intrinsic randomness as a measure of quantum coherence, Phys. Rev. A **92**, 022124 (2015).

[26] C. Napoli, T. R. Bromley, M. Cianciaruso, M. Piani, N. Johnston, and G. Adesso, Robustness of Coherence: An Operational and Observable Measure of Quantum Coherence, Phys. Rev. Lett. **116**, 150502 (2016).

[27] L. Li, Q. W. Wang, S. Q. Shen, and M. Li, Quantum coherence measurements based on Fisher information with applications, Phys. Rev. A **103**, 012401 (2021).

[28] H. Kwon, K. C. Tan, S. Choi, and H. Jeong, Quantum Fisher information on its own is not a valid measure of the coherence, Results Phys. **9**, 1594 (2018).

[29] A. B. A. Mohamed, E. M. Khalil, M. M. Selim, and H. Eleuch, Quantum Fisher information and Bures distance correlations of coupled two charge-qubits inside a coherent cavity with the intrinsic decoherence, Symmetry **13**, 352 (2021).

[30] R. S. Piera, S. P. Walborn, and G. H. Aguilar, Experimental demonstration of the advantage of using coherent measurements for phase estimation in the presence of depolarizing noise, Phys. Rev. A **103**, 012602 (2021).

[31] Z. Hradil, J. Řeháček, L. Sánchez-Soto, and B. G. Englert, Quantum Fisher information with coherence, Optica **6**, 1437 (2019).

[32] Z. H. Wang, W. Wu, G. D. Cui, and J. Wang, Coherence enhanced quantum metrology in a nonequilibrium optical molecule, New J. Phys. **20**, 033034 (2018).

[33] X. N. Feng and L. F. Wei, Quantifying quantum coherence with quantum Fisher information, Sci. Rep. **7**, 15492 (2017).

[34] Z. Liu, L. Qiu, and F. Pan, Enhancing quantum coherence and quantum Fisher information by quantum partially collapsing measurements, Quantum Inf. Process. **16**, 109 (2017).

[35] D. P. Lin, H. M. Zou, and J. H. Yang, Based-nonequilibrium-environment non-Markovianity, quantum Fisher information and quantum coherence, Phys. Scr. **95**, 015103 (2020).

[36] J. H. Yang, D. P. Lin, R. F. Liu, and H. M. Zou, Quantum Fisher information and coherence of an atom in a dissipative cavity, Laser Phys. **30**, 045202 (2020).

[37] C. W. Helstrom, *Quantum Detection and Estimation Theory* (Academic Press, New York, 1976).

[38] A. S. Holevo, *Probabilistic and Statistical Aspects of Quantum Theory* (North-Holland, Amsterdam, 1982).

[39] G. R. Jin and S. W. Kim, Spin squeezing and maximal-squeezing time, Phys. Rev. A **76**, 043621 (2007).

[40] A. Luati, Maximum Fisher information in mixed state quantum systems, Ann. Statist. **32**, 1770 (2004).

[41] J. Ma, Y. X. Huang, X. G. Wang, and C. P. Sun, Quantum Fisher information of the Greenberger-Horne-Zeilinger state in decoherence channels, Phys. Rev. A **84**, 022302 (2011).

[42] P. Hyllus, W. Laskowski, R. Krischek, C. Schwemmer, W. Wieezorek, H. Weinfurter, L. Pezzé, and A. Smerzi, Fisher information and multiparticle entanglement, Phys. Rev. A **85**, 022321 (2012).

[43] W. F. Liu, L. H. Zhang, and C. J. Li, Quantum Fisher information in two-qubit pure states, Int. J. Theor. Phys. **49**, 2463 (2010).

[44] M. A. Nielsen and I. L. Chuang, *Quantum Computation and Quantum Information* (Cambridge University Press, Cambridge, 2000).